Percolation of a fine particle in static granular beds

Song Gao (高颂),[1] Julio M. Ottino,[1,2,3] Paul B. Umbanhowar,[1] and Richard M. Lueptow[1,2,3,*]

[1] *Department of Mechanical Engineering, Northwestern University, Evanston, Illinois 60208, USA*
[2] *Department of Chemical and Biological Engineering, Northwestern University, Evanston, Illinois 60208, USA*
[3] *Northwestern Institute on Complex Systems (NICO), Northwestern University, Evanston, Illinois 60208, USA*

(Dated: March 20, 2023)

We study the percolation of a fine spherical particle under gravity in static randomly-packed large-particle beds with different packing densities ϕ and large to fine particle-size ratios R ranging from 4 to 7.5 using discrete element method simulations. The particle size ratio at the geometrical trapping threshold, defined by three touching large particles, $R_t = \sqrt{3}/(2-\sqrt{3}) = 6.464$, divides percolation behavior into passing and trapping regimes. However, the mean percolation velocity and diffusion of untrapped fine particles, which depend on both R and ϕ, are similar in both regimes, and can be collapsed over a range of R and ϕ with the appropriate scaling. An empirical relationship for the local percolation velocity based on the local pore throat to fine particle size ratio and packing density is obtained, which is valid for the full range of size ratio and packing density we study. Similarly in the trapping regime, the probability for a fine particle to reach a given depth is well described by a simple statistical model. Finally, the percolation velocity and fine particle diffusion are found to decrease with increasing restitution coefficient.

I. INTRODUCTION

Understanding flowing granular materials is of great importance for industrial applications in pharmaceutical, chemical, and agricultural production as well as for various geophysical processes [1, 2]. When granular materials differ in size, density, or other physical properties, segregation can occur, which in turn alters flow properties and can negatively affect industrial operations. In recent decades, numerous experimental, numerical, and theoretical studies have been conducted to interpret and model granular segregation [3, 4], with size segregation drawing the most attention. Size-driven segregation can be divided into two regimes depending on the relative sizes of the particles. When large and small particles have a size ratio less than about 3, a shear-induced size segregation mechanism captures the underlying physics. Small particles tend to percolate downward under the action of gravity through the spaces between large particles generated as the mixture is sheared due to flow [5–7]. However for larger size ratios, where we refer to the smaller particles as "*fine particles*," the relationship between the concentration dependent segregation velocity (or, equivalently, the flux) and the size ratio changes significantly. Specifically, the propensity for segregation increases with increasing particle size ratio when $R \lesssim 3$, but is nearly independent of size ratio when $R \gtrsim 3$ [8], where $R = d_l/d_f$ is the ratio of the large particle diameter, d_l, to the fine particle diameter, d_f. This behavior has been attributed to an increasing tendency toward free sifting, or spontaneous percolation, which occurs when the fine particles are small enough to pass through the voids between large particles even when the large particles are stationary.

Fine particles appear in industrial solids handling processes for various reasons, including particle attrition or the addition of free-flow agents. Unfavorable free sifting of fine particles can result in degraded product quality, fouled equipment, health risks like inhalation of fine particles, and safety hazards such as dust explosions [9, 10]. Fine particles also play important roles in geophysical flows. For example, they can act as bearing balls in long-runout landslides when they percolate to the bottom of the flow during the early phase of the landslide, thereby increasing the mobility of the overlying bed of particles during the later phase of the landslide [11–13]. However compared to the extensive number of studies on shear-induced segregation for size ratio less than three, few studies have focused on the free sifting problem, especially when the particle size ratio is below the geometric trapping threshold.

Central to understanding free sifting is identifying the particle size ratio above which fine particles freely pass through the smallest possible voids between static large particles. Dodds [14] considers this problem in detail based on the porosity of random sphere packings. The most restrictive passage is generated when three large particles form a triangle as shown in Fig. 1. The size ratio of the large sphere diameter to the diameter of the largest fine that can pass through the *"pore throat"* of this triangle is $R_t = d_l/d_p = \sqrt{3}/(2-\sqrt{3}) = 6.464$, where d_p is the pore throat diameter. This size ratio is called the geometrical trapping threshold [15, 16]. Numerical and experimental studies conducted after the work of Dodds [14] show that the analogous size ratio for a static randomly-packed large particle bed is about 6.67, which is slightly larger than R_t due to the occasional formation of jammed arches of fine particles between large particles [17, 18]. Similarly, for deep bed filtration, where multiple fine particles in suspension are

* r-lueptow@northwestern.edu

captured by a granular bed, the particle size ratio at the filtration threshold is about 6.62 [19], which again is slightly larger than R_t. Here we intentionally avoid the problem of clogging and jammed arches by considering single fine particles rather than multiple fine particles percolating simultaneously through the static bed.

Nevertheless, the dynamics of free sifting when the particle size ratio is close to and even below R_t has been largely ignored in previous studies on fine particle percolation in dry static granular beds driven by gravity, which either focus on free sifting of fine particles with $R > R_t$ [15, 16, 20–28], or explore the geometrical trapping threshold for randomly-packed beds [17, 18], as indicated by the key parameters of previous studies summarized in Table I. Following the pioneering work of Bridgwater *et al.* [20] and Bridgwater and Ingram [21], the majority of studies, both experimental and computational, have investigated the percolation velocity, diffusion, and residence time of fine particles falling through a static bed of larger particles as a function of particle size ratio, the number of fine particles, system dimensions, inter-particle restitution coefficient e, and friction coefficient μ for particle size ratio R much larger than R_t. The main conclusions of these studies are that fine particles exhibit a constant percolation velocity in steady state and that the dispersion of fine particles, both perpendicular and parallel to the direction of gravity, is diffusive [15, 16, 20–28]. Moreover, the concentration of fine particles affects the percolation velocity and particle dispersion, as fine-fine particle interactions are pronounced when concentration is high. Consequently, clogging or jamming of fine particles in a pore throat may hinder free sifting [16–18, 28].

TABLE I. Parameters in studies of free sifting of fine particles in static beds

Reference	R	ϕ	e
Rahman *et al.* [25]	14.7-10^3	0.494-0.527	0.3-0.9
Zhu *et al.* [26]	10-10^3	0.622	0.1-0.5
Richard *et al.* [23][a]	10	0.62-0.64	0.87-0.97
Bridgwater *et al.* [20][a]	8.8-28.5	0.63	0.2-0.92
Ippolito *et al.* [15][a]	8.6-22.9	0.55-0.59	n.s.[b]
Remond [28]	8-12.5	0.573	n.s.[b]
Bridgwater & Ingram [21][a]	7.4-45.5	0.63	0.2-0.92
Li *et al.* [27]	6.7-10^3	0.58	0.1-0.95
Lominé & Oger [24][a]	6.5-16	≈ 0.6	0.74-0.94
Lominé & Oger [16][a]	R_t-20	≈ 0.6	0.6-0.99
Kerimov *et al.* [18]	3.3-10^2	0.609-0.625	0.3
Roozbahani *et al.* [17]	2-20	0.581	n.s.[b]

[a] experimental results
[b] not specified

Although free sifting is usually thought to be significant only for size ratios larger than the geometrical trapping threshold in static large-particle beds, it has been hypothesized to be important in flowing beds even for $R < R_t$ [8]. Hence, to provide a basis for the study of free sifting in flowing granular materials, here we study

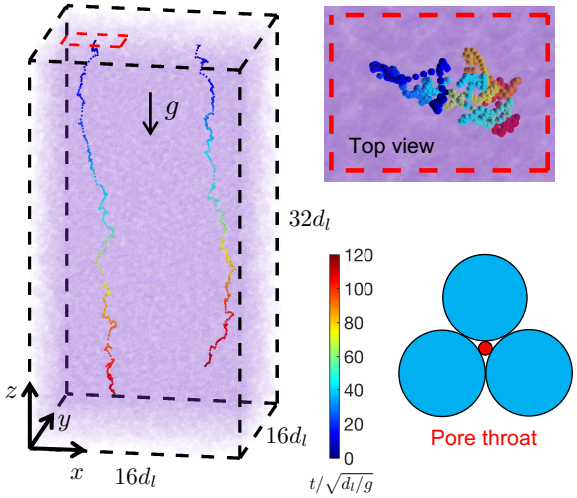

FIG. 1. (left) Perspective view of computational box and two representative fine particle trajectories (sampled at 5 ms intervals) in the free sifting regime ($R = 6.5$) for a static large-particle bed with $\phi = 0.577$. color map indicates dimensionless time, $t/\sqrt{d_l/g}$, during the trajectory. (upper-right) Top view of the trajectory of one particle. (bottom-right) Pore throat with a fine particle (red) at the geometrical trapping threshold limit.

the simpler problem of free sifting of a fine particle in random static packings of large particles for an intermediate size ratio range $4 \leqslant R \leqslant 7.5$. We consider packing densities from $\phi = 0.526$ to 0.639 over a wide range of restitution coefficients using discrete element method (DEM) simulations [29]. The particle size ratio range we consider encompasses the geometrical trapping threshold $R_t = 6.464$, such that both the passing and trapping regimes of the fine particles are investigated. We focus on the dynamic features of fine particle percolation through a bed of static large particles, namely the percolation velocity and fine particle diffusion coefficient in both the passing and trapping regimes. The structure of the random packings is characterized using the Delaunay triangulation method [30–33] in order to relate it to how far and how fast fine particles percolate through a packed bed.

The remainder of the paper is organized as follows. Section II describes our numerical simulations and provides an overview of the procedures for generating three-dimensional random packings of spherical particles with different packing densities. Section III characterizes the fine particle percolation velocity and diffusion in both the passing and trapping regimes, as well as the effects of the restitution and friction coefficients. This section also describes a pore-throat size distribution based statistical model that is used to predict the depth to which fine particles percolate in the trapping regime as well as a local percolation velocity based on the pore-throat size and packing density. Section IV summarizes our findings.

II. METHODS

A. Numerical simulations

Following a standard soft-sphere DEM approach for simulating granular materials [29], we study free sifting using our in-house DEM code [34], which runs on CUDA-enabled GPUs and has been previously validated by experiments with millimeter-sized glass spheres [34, 35]. For all simulations, a linear spring-dashpot model with Coulomb friction and rolling friction (simulation details are provided elsewhere [35]) determines particle-particle contact forces using a sliding friction coefficient of $\mu = 0.5$, a rolling friction μ_f related to the fine particle diameter as $\mu_r = 0.001 d_f$, a restitution coefficient of $e = 0.8$ (unless otherwise stated), and a binary collision time of $t_c = 10^{-4}\,\mathrm{s}$. As we will show in Sec. III F, the restitution coefficient affects the dynamics of free sifting significantly. To fully resolve particle collisions, the DEM simulation time step is $t_c/50$. Particle density is $2500\,\mathrm{kg\,m^{-3}}$ for both fine and large particle species.

The computational domain is shown in Fig. 1. We generate a random packing of large bed particles with identical diameter $d_l = 4\,\mathrm{mm}$ (details described in Sec. II B) in a $16d_l \times 16d_l \times 32d_l$ rectangular prism. The large particle diameter remains constant for all simulations unless otherwise noted. To eliminate wall effects [36, 37], all six bounding planes are periodic. Depending on the packing density, the number of large particles in the bed varies from 8,192 to 9,984. After a packed bed is formed, the bed particle positions are fixed to keep the structure unchanged. Then, 10^4 fine particles (diameter d_f) are randomly positioned in a horizontal plane at $z = 32.5d_l$ to avoid overlapping any large bed particles. Individual fine particles with zero initial velocity fall freely under gravity, in this case $g = 9.81\,\mathrm{m\,s^{-2}}$, although the influence of the magnitude of g is removed via a simple rescaling) [21]. The periodicity of the top and bottom boundaries is removed during the initialization and release of the fine particles, but is then restored after all fine particles have entered the bed. Consequently, fine particles that percolate down to $z = 0$ re-enter the fixed bed at $z = 32d_l$. Figure 1 demonstrates the trajectories of two fine particles in the static bed. Each fine particle percolates along an irregular path due to the random bed particle structure and collisional interactions with the bed particles.

Previous studies demonstrate that collective interactions among percolating fine particles may clog some pores of the granular bed, which can stop the flow even in the free sifting regime [16–18, 28]. In order to avoid this effect here, fine particles do not interact with each other, i.e. they are independent intruders. As a result, the dynamics of 10^4 independent intruder fine particles are simultaneously computed in one simulation, which is computationally efficient and provides sufficient data for accurate statistics in most cases. Thus, our results can be compared with previous studies in which the fine particle concentration is low enough that fine-fine particle interactions are unimportant.

B. Static bed preparation

We create random packings with different packing densities ϕ using a particle growth algorithm proposed by Lubachevsky and Stillinger [38] in order to characterize how the structure of the static large particle bed influences free sifting. This method can generate homogenous disordered packings over a range of packing densities up to the random close packing limit of $\phi \approx 0.64$ [39, 40]. Since the volume of the rectangular domain is constant, random packings with a wide range of packing density can be prepared by varying the number of bed particles. First, bed particles with a reduced initial diameter are randomly generated in the rectangular computational domain. The initial bed particle diameter is typically 3.5 mm, which is smaller than the final diameter of $d_l = 4\,\mathrm{mm}$. In order to establish homogeneous random packings, all boundaries are periodic, gravity is turned off during the expansion process, and inter-particle interactions are perfectly elastic. To achieve the desired packing density, bed particle diameter is grown slowly over 5 s with decreasing radial velocity, i.e. $d_l = 4 - 0.5e^{-t}$, after which d_l is directly set to 4 mm. As bed particles expand, interactions between them become more energetic and frequent as they increasingly overlap momentarily after growing. To minimize the degree of overlap and reduce the non-physical kinetic and collisional potential energy caused by the overlap, a relaxation process is applied in which the bed particle velocities are reset to zero [38]. The relaxation is conducted every 0.1 s until the desired large particle size and packing density are reached. Finally, the bed particles are allowed to relax for the last time with gravity off and collisional dissipation on to achieve a state of equilibrium (zero net kinetic and collisional potential energy within the numerical error), and then frozen in place. With this procedure, we obtain homogeneous random packings (no crystalline structures observed) with $0.526 \leqslant \phi \leqslant 0.639$. Particle overlap even at the highest ϕ is minimal: less than 0.1% of contacts overlap by more than 2.5% after the last relaxation. We note that mean packing densities with $\phi < 0.55$ are likely not mechanically stable under gravity for frictional non-cohesive particles [41], although packing densities as low as $\phi = 0.54$ may occur locally [42, 43]. Here, simulating packing densities slightly below this limit is useful to better understand the effect of the large particle bed structure on free sifting. We also note, and show later, that other methods of preparing static beds, e.g., pluviation, may alter the bed packing structure but do not change our key results showing how bed structural information can be used to determine percolation velocity and percolation depth.

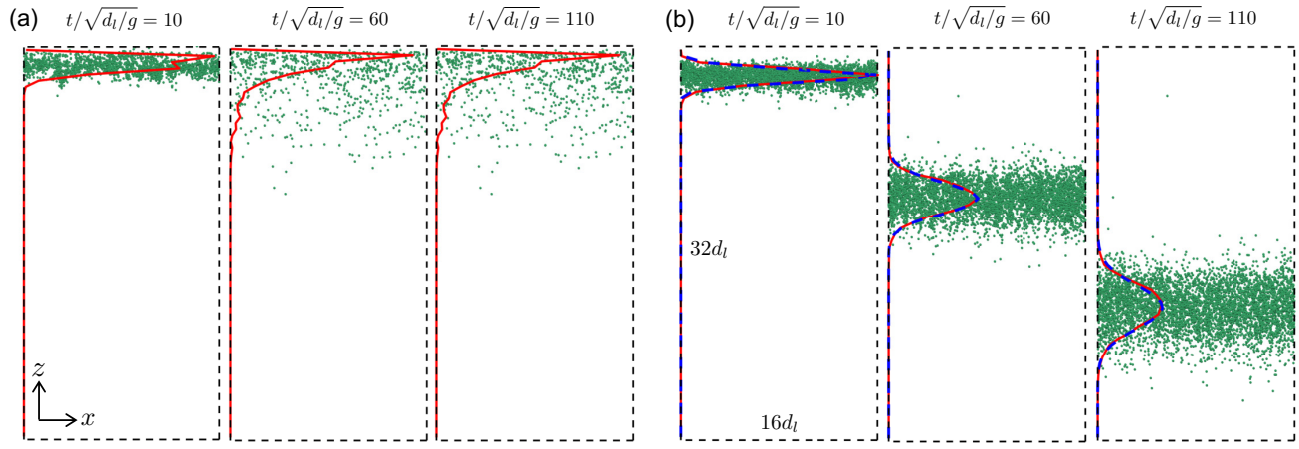

FIG. 2. Positions of 10^4 non-interacting fine particles in the xz-plane at different times for packing density $\phi = 0.639$ in (a) the trapping regime ($R = 5$), and (b) the passing regime ($R = 6.5$). Black dashed outlines are the fully-periodic boundaries of the computational domain in the xz-plane; large particles are omitted for clarity. Red curves indicate the fine particle number distributions vs. depth, and blue dashed curves in (b) are fits to a normal distribution.

III. RESULTS

A. Passing and trapping regimes

We begin by illustrating the two regimes of fine particle motion in a bed of large particles based on the geometrical trapping threshold, $R_t = 6.464$ [14]. Figure 2(a) shows the positions of 10^4 independent fine particles at various times for $R = 5 < R_t$, i.e., the fine particles are larger than the smallest pore throats that can be formed by a static bed and will eventually become trapped. The initial entrance time of a fine particle into the static bed, $t = 0$, is defined as the moment its z-position is $1.5d_l$ lower than the center of the highest bed particle for the remainder of the simulation to avoid including initial rebounds of fine particles above the free surface. As indicated by the fine particle number distributions (red curves) and positions, some fine particles percolate as far as $12d_l$ into the bed, although the majority are within $4d_l$ of the surface after all motion has ended by $t/\sqrt{d_l/g} = 110$. We call this the trapping regime—fine particles travel different distances before they finally cease percolating.

Contrast the trapping regime with the situation shown in Fig. 2(b) for $R = 6.5$, which is only slightly larger than $R_t = 6.464$. Since every fine particle is smaller than the smallest possible pore throat, none become trapped in pore throats as they percolate downward with a constant average percolation velocity. We call this the passing regime. Due to the stochastic nature of fine particle trajectories in the passing regime, vertical dispersion increases in time as is evident from the broadening of the particle number distributions (red solid curves), which are well fit by normal distributions (blue dashed curves). Both the vertical and the horizontal dispersion is diffusive, as we characterize in detail later in this section.

We note that in the passing regime a small number of fine particles (typically less than 0.05%) can move very slowly or stop moving entirely, e.g., the three green dots in the upper-half of the domain for $t/\sqrt{d_l/g} = 110$, despite the fact that our DEM contact model precludes permanently stationary particles in the passing regime (where there is a maximum of two point contact between fine and bed particles) due to its lack of static rolling friction. In our simulations, both slowly moving and stopped fine particles are associated with trajectories that impact a bed sphere near its apex with small horizontal velocity. The former become effectively trapped over the finite duration of our simulations as they slowly roll down from the bed sphere apex, while the latter are permanently stopped because the computed changes in position (linear and angular) are all smaller than the numerical resolution of the corresponding variables, i.e. particle position remains constant. Of course in physical experiments, permanently stationary particles are possible even for $R > R_t$ due to particle imperfections (e.g., flats and asperities) and cohesive interactions. In our simulations, however, permanently stopped particles have negligible influence on our results due to their very small relative numbers.

B. Percolation velocity

As shown in Fig.1, fine particles primarily move down in the static bed following a random route in both vertical and horizontal directions due to collisions with large particles in the bed. Consider first the passing regime, where a steady mean percolation velocity is quickly achieved [15, 16, 20, 21, 23, 24, 26, 27]. Here, we consider the vertical displacement of each particle Δz over a

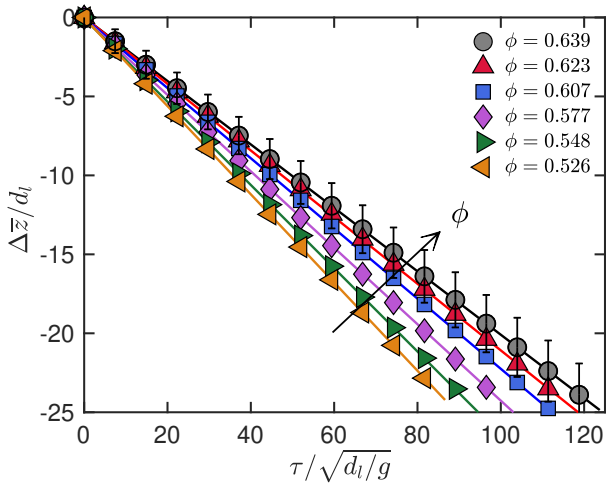

FIG. 3. Passing regime: non-dimensional mean vertical displacement vs. non-dimensional time interval for fine particles with $R = 7$ at various ϕ.

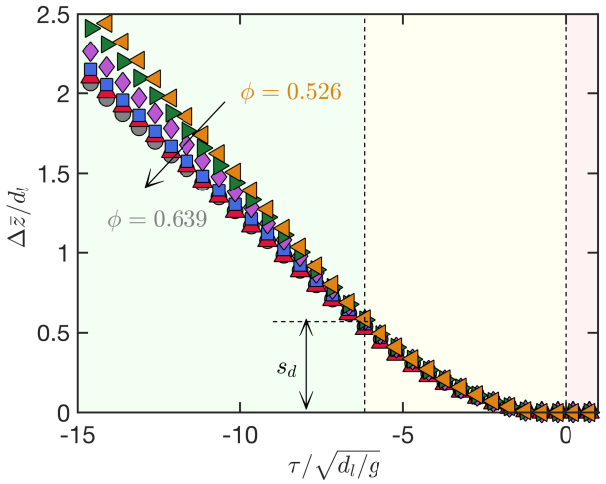

FIG. 4. Trapping regime: conditionally averaged non-dimensional mean vertical displacement vs. non-dimensional time interval with respect to trapping time for fine particles with $R = 5$ at different ϕ. Symbols are defined in Fig 3. The three regions show where fine particles percolate at a constant velocity (green), decelerate (yellow), and stop (red). Stopping distance, s_d, is the vertical distance over which fine particles slow to a stop.

time interval τ starting after it enters the static bed (to avoid inconsistencies due to fine particles entering the static bed at different initial times or bouncing above the top of the static bed before entering it). The average non-dimensional vertical displacement of all fine particles, $\Delta\bar{z}/d_l$, versus the non-dimensional time, $\tau/\sqrt{d_l/g}$, for $R = 7$ is plotted in Fig. 3. The percolation velocity, which is the local slope of each curve, $v_p = \Delta\bar{z}/\tau$, is essentially constant for each packing density, ϕ, consistent with previous studies for fine particles with $R > R_t$, and decreases as packing density increases, as expected. The uncertainty bars, shown only for $\phi = 0.639$ for clarity, increase with time, consistent with the increasing vertical dispersion of fine particles evident in Fig. 2(b). Similar results are found for other size ratios with $R > R_t$.

In the trapping regime, all fine particles eventually stop (all simulations run for sufficient time to ensure that more than 99.95% of the fine particles stop percolating), but they stop at different instants. Consequently, there are always two populations of fine particles in the trapping regime at any particular time before all fine particles stop, i.e., some are moving while the others have been trapped. To accurately capture and demonstrate the transient dynamics of fine particles before they cease percolating, we use a conditional averaging approach. The vertical positions of fine particles over a time interval of $\tau/\sqrt{d_l/g} = 15$ before they stop are offset and aligned according to their final positions, which are set to zero at $\tau = 0$. The conditionally averaged data are shown in Fig. 4 for $R = 5$ and various ϕ. There are three sequential temporal regions: in the green region, fine particles pass through the large particle bed at a constant average percolation velocity (as indicated by the slope) just as observed in the passing regime, even though their size ratio is larger than R_t; in the yellow region fine particles slow down; in the red region, particles are no longer moving. Therefore, even in the trapping regime a percolation velocity can be obtained prior to when the fine particles slow down and stop. Similar to the passing regime, the percolation velocity decreases as ϕ increases. Interestingly, the stopping distance, s_d, defined as the distance from where the data first deviate from linear (where the local gradient is 5% smaller than that of the linear portion in the green regime) to the trapped depth, is nearly the same for all ϕ with a value of $s_d \approx 0.55 d_l$, see Fig. 4. This indicates that the trapping region is smaller than the static bed particle but essentially independent of ϕ, at least for the packing densities considered here. s_d decreases by less than about 10% when particle size ratio is decreased from 6 to 4, which is surprisingly small, but the decrease is consistent with the fact that larger fine particles ($R = 4$) have less free space to move within the packed bed.

We now compare the percolation velocity for both the trapping and passing regimes for various R and ϕ based on the slopes of the displacement versus time data using only the portion of the fine particle trajectories where the slope of Δz vs. τ is linear (green region in Fig. 4). As shown in Fig. 5(a), the previously proposed dimensionless percolation velocity, $v_p/\sqrt{gd_l}$ [21], for a fixed R decreases nearly linearly as ϕ increases since denser packing increasingly constrains the movement of the fine particles. For constant ϕ, v_p increases as R increases because fine particles are smaller compared to the bed large particle (previous studies showed that the percolation velocity asymptotically approaches a maximum as R is further increased [25, 27]). Perhaps more importantly, the percolation velocity is similar for both the passing and trapping

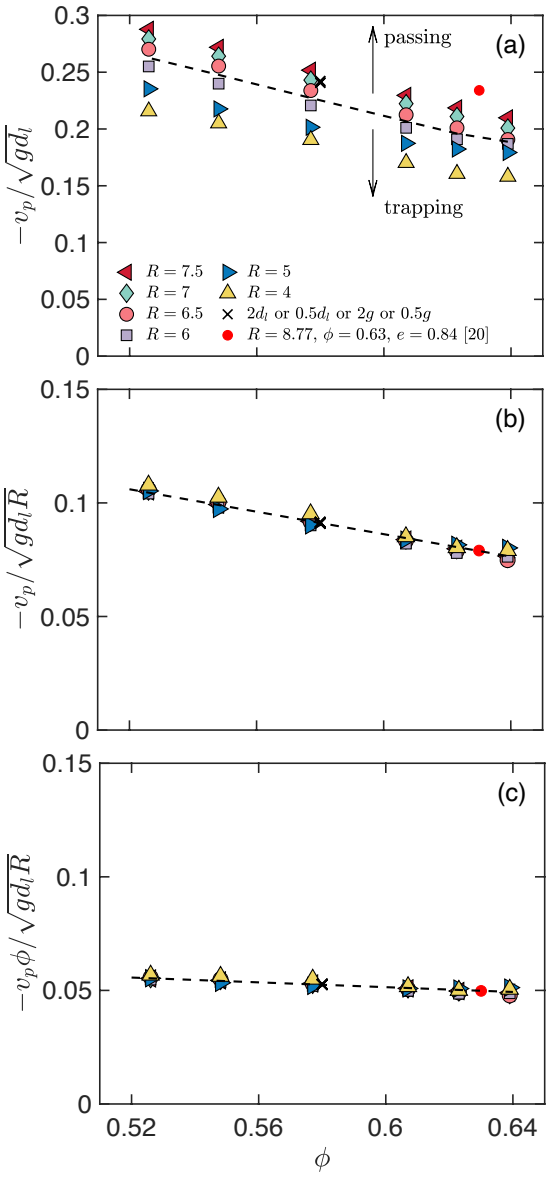

FIG. 5. (a) Non-dimensional percolation velocity $v_p/\sqrt{gd_l}$ vs. packing density ϕ for various R across the passing and trapping regimes for restitution coefficient $e = 0.8$. The dashed curve approximates the boundary between the passing (above) and trapping (below) regimes. (b) Scaling the non-dimensional percolation velocity by $\sqrt{R}$ removes the R dependence. (c) Scaling the non-dimensional percolation velocity using both R and ϕ makes it nearly constant. Data points for $R = 7$ and $\phi = 0.577$ at different simulation conditions (black $\times$) are offset slightly to the right to make them more visible. In (b) and (c), the dashed line is a linear fit to the data.

regimes from two standpoints. First, the dependence of v_p on R and ϕ, is similar in both cases. Second, there is a smooth decrease in v_p from the trapping regime to the passing regime, rather than a sudden jump, even for the condition where ϕ approaches the random close packing limit ($\phi \approx 0.64$). To check that the results in Fig. 5(a) are independent of the specific values of g and d_l primarily considered here, we perform additional simulations for $R = 7$ and $\phi = 0.577$ that are identical except with large particle diameters of $0.5d_l$ or $2d_l$ or with gravitational accelerations of $0.5g$ or $2g$. Results for these four cases [black crosses in Fig. 5(a)] almost overlap one another as well as the data point for 4 mm large particles at g, indicating that v_p scales as $\sqrt{gd_l}$, which reflects the free fall velocity of a particle over a distance that scales with the large particle diameter, d_l, i.e., the pore diameter [15]. Moreover, our simulation results are consistent with a previous experimental result (small red filled circle in Fig. 5(a) [21]), accounting for its size ratio being larger ($R = 8.77$) than those considered here.

Although the geometrical trapping threshold, $R_t = 6.464$, effectively determines whether a fine particle is ultimately trapped or not, R_t is not a sharp threshold for delineating the dynamics of free sifting in a randomly-packed bed. That is, fine particles can traverse a significant distance at a significant percolation velocity through a bed of static large particles for R well below the geometrical trapping threshold, R_t, in random packings. This may have significant implications for free sifting in flowing granular mixtures, where it is not only the particle size ratio that determines when free sifting occurs, but also the nature of the flow, which alters the packing density and causes voids between large particles to continually open up as particles flow. While flowing large particles are beyond the scope of this paper, the similarity of results below and above R_t in Fig. 5(a) suggests that the observed change in the percolation of small particles in granular flows for $R > 3$ is indeed likely a consequence of the increasing significance of free sifting with increasing R, as previously suggested [8].

The similar dependence of the percolation velocity on size ratio and packing density suggests scaling the percolation velocity by those parameters. We have considered several ways to scale the percolation velocity and found that using $\sqrt{gd_lR}$ (equivalent to $d_l\sqrt{g/d_f}$) best collapses the data for all R tested, as shown in Fig. 5(b). The origin of this scaling is unclear. It is the ratio of the time scale for a fine particle to fall a distance equal to its diameter, $\sqrt{d_f/g}$, to the time scale to traverse the length of a pore at the mean percolation velocity, d_l/v_p (noting that the pore size scales with d_l). And while this scaling also works for a previous experimental result at larger R than we consider here (small red circle [21]), it cannot be the correct scaling in the limit of large R where the percolation velocity eventually plateaus for $R \gtrsim 30$ [27].

The data can be further collapsed to a nearly constant value of $\approx$0.05 by multiplying $v_p/\sqrt{gd_lR}$ by ϕ, see Fig. 5(c). Thus, the scaled fine-particle percolation velocity in static randomly-packed beds, $v_p\phi/\sqrt{gd_lR}$, is a constant in both the passing and trapping regimes for $4 \leq R \lesssim 9$ and packing densities ranging from slightly below the lower limit for frictionally-stabilized random packing [41] to random close packing ($0.526 \leqslant \phi \leqslant 0.639$). The scaled value of v_p (here 0.05 for $e = 0.8$) is resti-

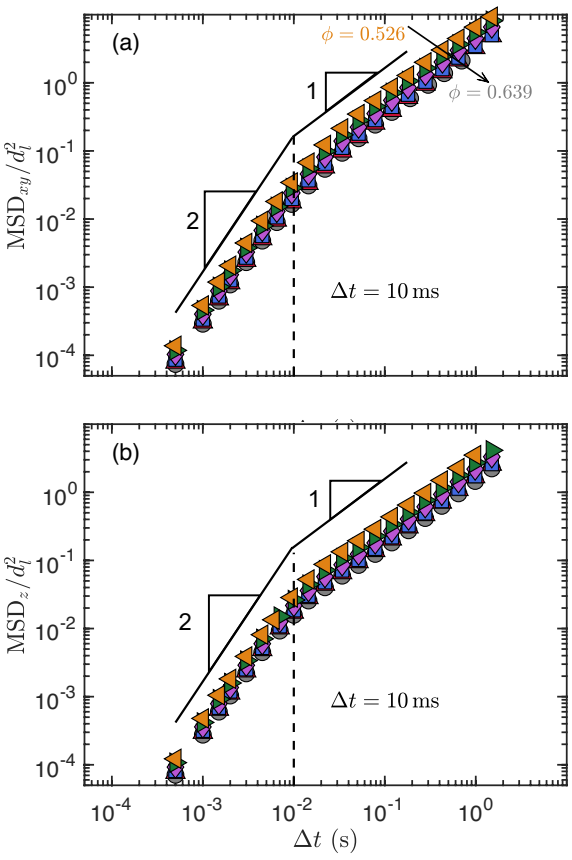

FIG. 6. Non-dimensional mean squared displacement (MSD) of fine particles vs. time interval Δt in the passing regime ($R = 7$): (a) projected to the xy-plane (horizontal) and (b) in the z-direction (vertical). Results for various ϕ are shown, and symbols are defined in Fig. 3.

tution coefficient dependent as discussed below in the context of Figs. 7 and 15.

C. Fine particle diffusion

In the passing regime, the percolation of a fine particle is essentially a random walk (biased in the vertical direction), as is evident in the trajectories shown in Fig. 1. Such random motion leads to position dispersion of percolating fine particles in the packed bed, both in the horizontal and vertical directions [15, 16, 20, 21, 24–27]. To quantify the dispersion, the mean squared displacement (MSD) of all fine particle trajectories is measured. In the horizontal direction, i.e., the xy-plane, the two-dimensional MSD is calculated as

$$\mathrm{MSD}_{xy}(\Delta t) = \langle \Delta X(\Delta t)^2 + \Delta Y(\Delta t)^2 \rangle, \qquad (1)$$

where $\Delta X(\Delta t) = x(t_0 + \Delta t) - x(t_0)$ and $\Delta Y(\Delta t) = y(t_0 + \Delta t) - y(t_0)$ are the displacements in the $x-$ and $y-$directions, respectively. The angled brackets represent the averages over all particles and over different values of t_0 after the steady percolation state is achieved. In the vertical direction (z-direction), the diffusion process occurs with respect to a mean flow, so the MSD is calculated as [44]

$$\mathrm{MSD}_z(\Delta t) = \langle [z(t_0 + \Delta t) - z(t_0) - v_p \Delta t]^2 \rangle, \qquad (2)$$

where $v_p \Delta t$ is the mean displacement of fine particles in the z-direction over the time interval Δt. As shown in Fig. 6, MSD_{xy} and MSD_z both display a transition from a short-time-interval ballistic regime with slope of approximately 2 [45] to a long-time-interval normal diffusive regime with slope of approximately 1 [46]. For $\phi = 0.526$, the slope transitions occur at $\Delta t \approx 10\,\mathrm{ms}$ for both MSD_{xy} and MSD_z, which is about the average free flight time of fine particles between collisions with large particles [45]. The time interval also indicates the size of the structural constraint of random packings, which is on the order of $0.1 d_l$. Finally, the time scale decreases by less than 10% as ϕ increases to 0.639.

The diffusion coefficients, which are based on $\mathrm{MSD}_{xy} = 4 D_{xy} \Delta t$ and $\mathrm{MSD}_z = 2 D_z \Delta t$ [47], respectively, are determined by fitting the linear portion (with slope of 1) of the MSD curves in Fig. 6. For the trapping regime, we consider only the portion of the fine particle trajectories for which the fine particles pass through the large particle bed at a constant percolation velocity (green region in Fig. 4). The diffusion coefficient, non-dimensionalized by $\sqrt{g d_l^3}$ based on the assumption that it scales with the space between the large bed particles, is plotted for various packing densities and size ratios in Figs. 7(a) and 7(d). We omit the results for $R = 4$, and $R = 5$ for $\phi > 0.577$, because fine particles are trapped quickly in these situations, hindering the accumulation of sufficient data to accurately evaluate the MSD at the time intervals of interest. As would be expected, for a fixed size ratio, the diffusion coefficient decreases as packing density increases, consistent with a previous study [22]. And for a fixed packing density, smaller size ratios have a smaller diffusion coefficient because the motion of larger fine particles is more constrained by the static packing. As was the case for the percolation velocities, no sharp distinction exists between the diffusion coefficients in the passing regime versus the trapping regime. D_{xy} from an earlier study with $\phi = 0.6$ and $R = 7.5$ [16] [solid red circle in Fig. 7(a)] is lower than our closest corresponding result, but is nevertheless consistent with our results. Again, varying the large particle size and the gravitational acceleration gives results that are nearly identical (black crosses).

We additionally consider two alternative scaling approaches for D_{xy} and D_z. In Figs. 7(b) and 7(e), the diffusion coefficient is non-dimensionalized by $\sqrt{g d_l^3 R^3}$ (following the scaling of percolation velocity). Similar to the dimensionless percolation velocity in Fig 5(b), this scaling reduces the R dependence, particularly for larger values of ϕ, although the experimental data point for $R = 7.5$ does not collapse as well with our data. Using $\sqrt{g d_l^3 R}$ (again inspired by the scaling for the percola-

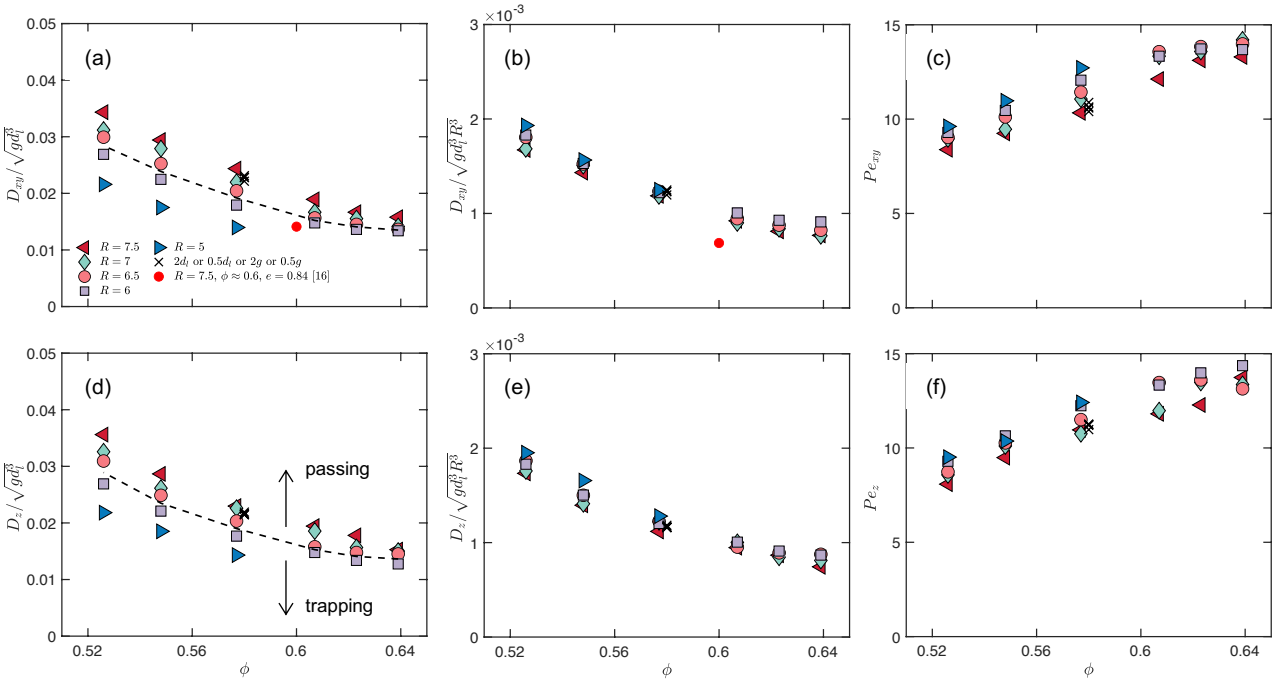

FIG. 7. Diffusion coefficient in the (a-c) xy-plane projection (horizontal) and (d-f) z-direction (vertical) scaled by (a,d) large particle diameter, $\sqrt{gd_l^3}$, (b,e) $\sqrt{gd_l^3R^3}$, and (c,f) expressed as Péclet numbers vs. packing density for various R in the passing and trapping regimes for restitution coefficient $e = 0.8$. Data symbols for $R = 7$ and $\phi = 0.577$ at different simulation conditions, as indicated in (a), are offset slightly to the right to make them more visible. Dashed curve in (a,d) approximates boundary between passing (above) and trapping (below) regimes.

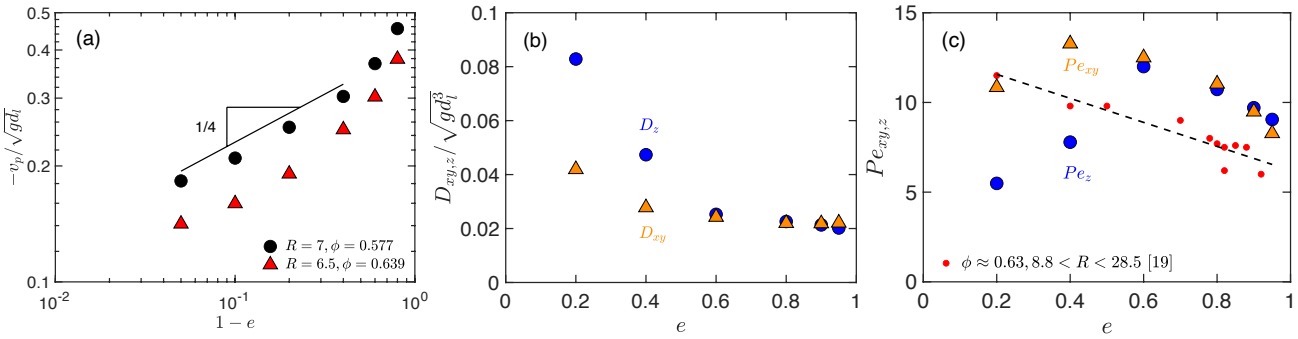

FIG. 8. Effects of restitution coefficient e in the passing regime on (a) percolation velocity, (b) diffusion coefficients and (c) Péclet numbers. Dashed black line is linear fit of experimental results for Pe_{xy} (small red filled circles) [20]. For (b) and (c), only results for $R = 7, \phi = 0.577$ are shown for clarity.

tion velocity) is less effective in collapsing the data (not shown), although the experimental data point is closer to our simulation results.

Finally, Bridgwater *et al.* [20] suggest using the Péclet number to describe the transport of fine particles in static beds. Figures 7(c) and 7(f) show the Péclet numbers, $Pe_{xy} = -v_p d_l / D_{xy}$ and $Pe_z = -v_p d_l / D_z$, for various R at various ϕ. Results for different size ratios collapse to some extent, although not as well as with the $\sqrt{gd_l^3R^3}$ scaling. Additionally, Pe increases sublinearly with ϕ, indicating that the percolation velocity decreases with ϕ more quickly than the diffusion coefficient. Furthermore, D_{xy} and D_z (similarly, Pe_{xy} and Pe_z) have similar values for the same R and ϕ, as observed experimentally [21], indicating that diffusion is similar for the horizontal and vertical directions, at least when $e = 0.8$.

D. Effects of restitution and friction coefficients

Up to this point, the restitution coefficient for particle collisions has been fixed at $e = 0.8$. However, the restitution coefficient affects both the percolation velocity and diffusion of free sifting significantly. We examine its in-

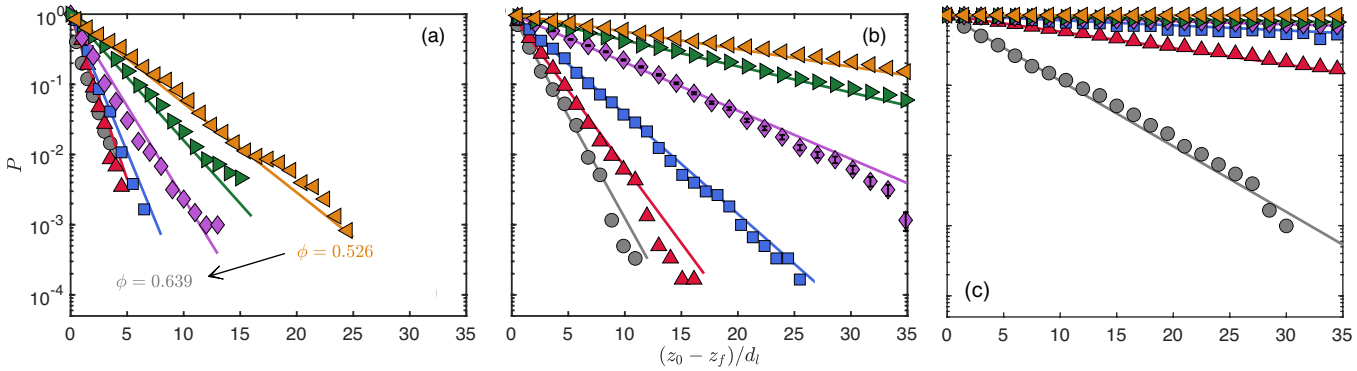

FIG. 9. Probability P in the trapping regime that a fine particle reaches scaled depth $(z_0 - z_f)/d_l$ for (a) $R = 4$, (b) $R = 5$, and (c) $R = 6$ for various ϕ (symbols defined in Fig. 3). Uncertainty bars plotted in (b) for $R = 5$, $\phi = 0.577$ are due to finite fine particle number (see text). Solid lines are model predictions using Eq. 4.

fluence in the passing regime for different ϕ and R, but similar results occur for the trapping regime. As shown in Fig. 8(a), for two pairs of R and ϕ values, the percolation velocity decreases by more than a factor of 2 with increasing restitution coefficient (from $e = 0.2$ to $e = 0.95$) as reported previously [15, 16, 20, 21, 24, 26]. The reason for this decrease is that less dissipative interactions between particles drive fine particles to rebound more energetically when colliding with bed particles, and, consequently, fine particles remain in the voids between bed particles for a longer time before falling into the next void. Moreover, the percolation velocity follows the relationship $v_p/\sqrt{gd_l} \propto (1 - e)^{1/4}$ for more elastic collisions ($e \geq 0.6$), consistent with a theoretical analysis for two-dimensional percolation based on an analysis of Brownian motion [48].

The influence of the restitution coefficient on the diffusion coefficients is more complicated, as shown in Fig. 8(b). For $e \geq 0.6$, both D_{xy} and D_z are nearly independent of e and have similar values, as found previously [16]. This may be understood by considering that a fine particle with higher e tends to bounce more times in a void between bed particles before passing through one of the void's pore throats. Thus, the fine particle is nearly as likely to exit the void either vertically or horizontally, yielding a similar degree of diffusion regardless of direction. For $e < 0.6$ and decreasing, however, D_z and D_{xy} increase significantly, with D_z increasing more than D_{xy}. The increase in D_z and D_{xy} with decreasing e is expected as diffusion tracks the response of v_p, which also increases with decreasing e and to which diffusion should be proportional [16]. The relatively larger increase in D_z relative to D_{xy} with decreasing e is apparently due to the larger increase in the width of the velocity distribution of the former. For instance, consider a fine particle falling toward a pore throat in the limit of $e = 0$. If its trajectory is aligned or nearly aligned with the center of the pore throat, few if any rebounds occur and its vertical velocity remains large. However, if it strikes a pore-throat constituent particle near its highest point, the fine particle vertical velocity will be reduced to nearly zero. In contrast to our results, however, a previous study finds that D_{xy} increases by about 40% as e is increased from 0.5 to 0.9 Zhu *et al.* [26]. This reversed result relative to our findings may be a consequence their approach, which considers interactions between fine particles, which we ignore, and uses different physical particle properties.

We also consider the impact of e on the Péclet number, shown in Fig. 8(c). Both Pe_z and Pe_{xy} decrease with increasing e for $e \geq 0.6$. The trend matches previous experiments for P_{xy} [20], as shown in the figure, although the experiments have somewhat smaller values, which may be a result of larger particle size ratios, $8.8 \leq R \leq 28.5$, interactions between fine particles, and details of how the diffusion coefficient was measured in the experiments. Nevertheless, the reasonably close match between the experiments and our simulations confirms the validity of our results for $e \geq 0.6$. Pe_z decreases significantly when $e < 0.6$ because of the more rapid increase of D_z compared to v_p with decreasing e.

Unlike the restitution coefficient, the friction coefficient has negligible influence on both percolation velocity and diffusion coefficients of free sifting when varied from $\mu = 0.2$ to 0.8. Low sensitivity to the friction coefficient value is also observed in simulations with fine particle concentrations below 10% [28].

E. Percolation depth in the trapping regime

Returning to the trapping regime, we use a simple approach to understand and predict the vertical distance that fine particles percolate before they are trapped. The probability, P, that a fine particle reaches a given depth z_f is obtained by calculating the fraction of the 10^4 fine particles that exceed this depth at the end of the simulation. All fine particles start at the free surface, z_0, so that $P = 1$ at dimensionless height $(z_0 - z_f)/d_l = 0$. P decreases as depth increases, indicating that fine particles have less chance to migrate deeper into the static bed.

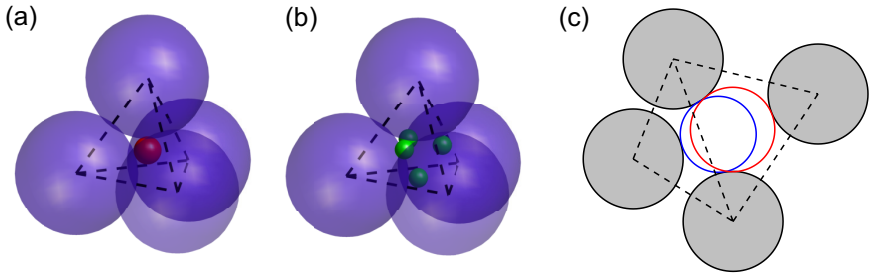

FIG. 10. (a) Red sphere inscribed in a tetrahedron formed from four large bed particles. (b) Four green spheres positioned at the narrowest point of each of the four pore throats of the tetrahedron indicate the maximum diameter of a passable fine particle. (c) Two-dimensional illustration of two Delaunay cells that can be merged (see text) [31, 32].

Figure 9 shows the probability P that a fine particle can reach a dimensionless displacement of $(z_0 - z_f)/d_l$ before it is trapped by the static bed for three different size ratios, with $R < R_t$, and various ϕ. For a given R, fine particles have a lower probability of traveling deeply into bed when the packing is denser. Conversely, for a given packing density ϕ, a larger size ratio R results in a higher chance for fine particles to percolate farther because they are smaller relative to the bed particle voids. Uncertainty bars [49], shown in Fig. 9(b) for one case, are typically smaller than the symbols but increase with depth because fewer fine particles can percolate more deeply in the bed, leading to larger uncertainty for the measured probability. Figure 9(c) shows that for $R = 6$ and $\phi < 0.6$, fine particles are rarely trapped and can percolate a long distance through the bed as indicated by the nearly horizontal data sets.

From Fig. 9, it is clear that the probability P decreases nearly linearly on the semi-logarithmic plot as a function of the non-dimensional percolation distance, i.e.,

$$\log P = k\frac{z_0 - z_f}{d_l}, \tag{3}$$

where k is the slope. Similar exponentially decreasing fine particle concentration with increasing percolation depth has also been observed in deep bed filtration [50, 51]. To model the trapping depth probability, we assume that the probability for a fine particle to pass through a randomly selected pore throat is P_p. Then, the probability to pass through n pore throats consecutively is ${P_p}^n$, assuming independent events. If the average vertical distance between pore throats along the fine particle trajectory is $\Delta\bar{z}_p$, then $n = (z_0 - z_f)/\Delta\bar{z}_p$, and the probability P for a fine particle to travel a distance of $z_0 - z_f$ can be expressed as,

$$P = P_p^{(z_0 - z_f)/\Delta\bar{z}_p}. \tag{4}$$

This expression can be rewritten as,

$$\log P = \frac{\log P_p}{\Delta\bar{z}_p/d_l}\frac{z_0 - z_f}{d_l}. \tag{5}$$

This relationship is analogous to a previous percolation model [52], but we additionally show that the slope in Fig. 9, $\log P_p/(\Delta\bar{z}_p/d_l)$, is determined by two physical parameters related to the structure of the packed bed, P_p and $\Delta\bar{z}_p$, both of which are measured by characterizing the pore-throat size distribution and the vertical spacing of the throats.

1. *Pore-throat diameter*

The Voronoi-Delaunay tessellation method and several variations on the method [53, 54] are commonly used to characterize the void structure in porous materials. Here, the standard Delaunay triangulation is a sufficient,

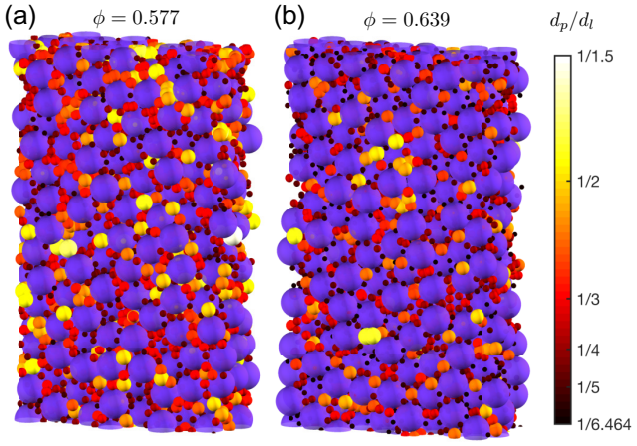

FIG. 11. Two randomly-packed large particle beds (purple spheres) and corresponding pore-throat spheres (color map indicates pore-throat size) obtained using the L1 method [32] for (a) $\phi = 0.577$ and (b) $\phi = 0.639$.

simple, and convenient option [30–33] that is based on sets of non-overlapping tetrahedrons whose vertices are the centers of four neighboring spherical particles, see Fig. 10(a). Once the packing is partitioned into tetrahedrons, the Apollonius approach [55] is implemented for each tetrahedron to obtain the largest pore sphere that can be placed inside the four particles [single red sphere in Fig. 10(a)] and the four pore-throat spheres [green in Fig. 10(b)], which represent the largest fine particle able to pass through each throat. For a regular tetrahedral arrangement of four identical large bed spheres that contact one another, the ratio of the large bed particle diameter to the pore sphere diameter (red) is $2/(\sqrt{6}-2) \approx 4.449$, and the ratio of the bed particle diameter to the pore-throat sphere diameter (green) is the geometrical trapping threshold, 6.464.

The triangulation process described above is denoted as Level 0 (L0) [32]. However, the L0 analysis is likely to generate inaccurate identification of pore-throat locations and sizes in disordered packings [31, 32]. The main reason is that a pore throat bounded by more than four bed particles, which frequently occurs in a random packing, cannot be appropriately captured by the L0 method, leading to the over-segmentation of a single large void space into several overlapping smaller void spaces; see, for example, the two-dimensional sketch in Fig. 10(c). To avoid this problem, Reboul *et al.* [32] suggest a Level 1 (L1) method to combine adjacent tetrahedra if they have overlapping pore throats, such as the blue and red circles in Fig. 10(c). Using the L1 method, a combined pore throat bounded by the four bed spheres [gray circles in Fig. 10(c)] can be found. If no analytical solution is possible, only the small blue pore throat is considered as the constraint for this combined pore space.

Since the pore-throat diameter is the length scale that determines whether a fine particle passes through the pore-throat or not, we use it to characterize the packing in the following analysis. Figure 11 shows the large bed particles (purple) and corresponding pore-throat spheres (color scale indicates pore-throat size) for two packing densities using the L1 approach. For the denser packing, the pore throats are smaller (darker), while for the looser packing the pore throats are larger (lighter). Note that the smallest pore throats have $d_p = d_l/6.464$, consistent with the value of R_t.

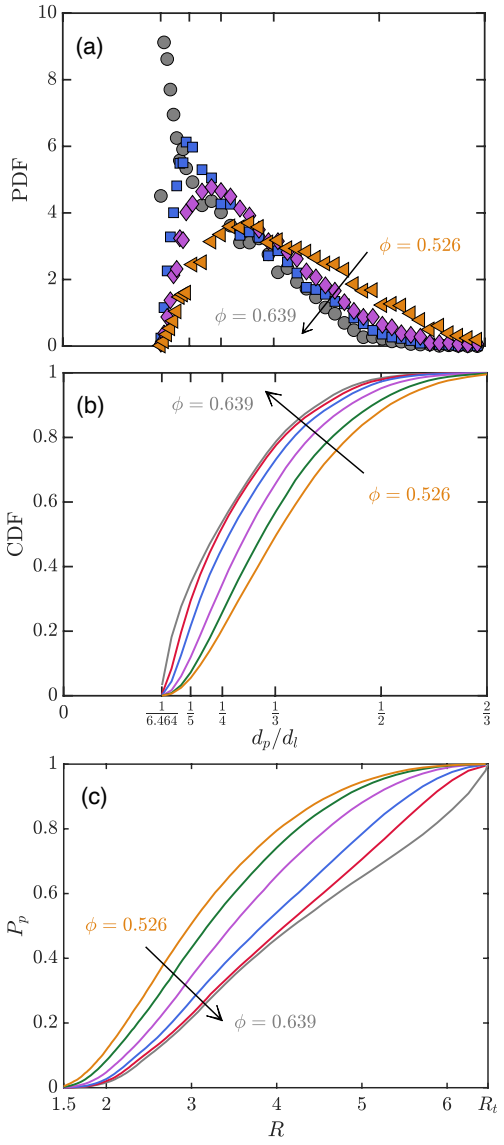

FIG. 12. (a) Pore-throat size distributions, (b) corresponding cumulative distribution functions (CDF), and (c) passing probabilities vs. $R = d_l/d_f$ for different ϕ. Color and corresponding ϕ values are as in Fig. 3, and only data for $\phi = 0.526, 0.577, 0.607$, and 0.639 are shown in (a) for clarity.

2. *Pore-throat size distribution*

Figure 12(a) shows the probability density function (PDF) of the pore-throat size for different bed packing densities using the L1 analysis. The minimum pore-throat size has a value of $d_p/d_l = 1/R_t = 1/6.464$. The maximum pore diameter depends on the packing density, which is $d_p/d_l = 2/3$ for the loosest random packing at $\phi = 0.526$, and decreases with increasing ϕ. When packing density is higher, the maximum in the PDF shifts toward the R_t limit because the denser packing generates more small pore throats. As packing density decreases, the peak moves away from the R_t limit, and the distribution is flatter. The pore-throat size distribution result for $\phi = 0.607$ (blue squares) is similar to previous results for $\phi \approx 0.6$, where the peak occurs at $d_p/d_l \approx 1/5$ and maximum pore-throat diameter is about $0.5d_l$ [32, 33]. The cumulative density function (CDF), which is the integral of the PDF with respect to d_p/d_l, is the fraction of pore throats with size ratio smaller than d_p/d_l. As shown in Fig. 12(b), for a given value of d_p/d_l, the CDF is larger for denser packing as it produces more small pore throats. The utility of the CDF here is that it

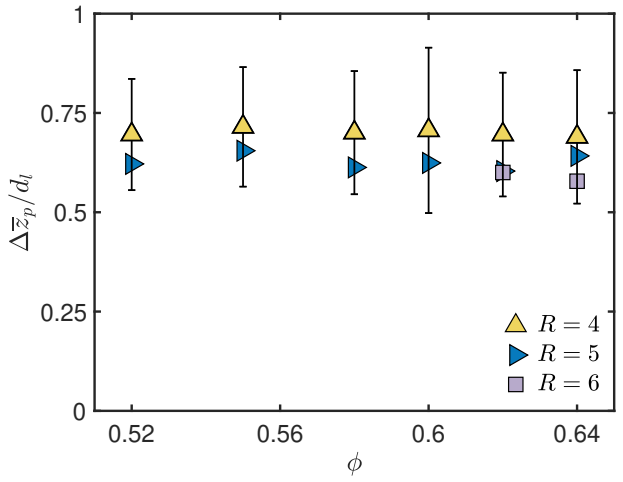

FIG. 13. Average vertical distance normalized by large particle diameter, $\Delta\bar{z}_p/d_l$, between passable pore throats on the paths of all fine particles for different particle size ratios R at different packing densities ϕ. Uncertainty bar depicting the standard deviation of the measurement is only shown for $R = 4$ for clarity.

can be used to obtain the passing probability P_p used in Eqs. 4 and 5: a fine particle of diameter d_f passes a random pore throat with passing probability P_p = 1-CDF($d_p/d_l = d_f/d_l$= $1/R$). P_p for fine particles with different particle size ratios in static packings with different packing densities is shown in Figure 12(c). Note the enhanced sensitivity of P_p to variation in ϕ at intermediate R, e.g., $P_p(R = 4, \phi = 0.526) \approx 2P_p(R = 4, \phi = 0.639)$.

3. *Average vertical distance between pore throats*

In addition to the pore-throat diameter, the other key physical property of the packed bed is the average vertical distance between pore throats, $\Delta\bar{z}_p$, along a fine particle trajectory, which is obtained by determining the pore throats that a fine particle passes through and averaging the vertical distance between pore throats over the trajectories of all fine particles. Figure 13 shows that for any given packing density, $\Delta\bar{z}_p$ decreases with increasing R, indicating that the average distance between accessible pore throats decreases, as would be expected. Interestingly, for a particular size ratio R, $\Delta\bar{z}_p$ remains nearly unchanged for various ϕ. This likely occurs because for a fine particle with a fixed size, the number of passable pore throats decreases for a denser packing (i.e., $\Delta\bar{z}_p$ should increase), but a denser packing results in the reduction of the average distance between bed particles, and accordingly a reduction in the average distance between pore throats (i.e., $\Delta\bar{z}_p$ should decrease). Conversely, for a looser packing more pore throats are passable but the average vertical distance between all pore throats is larger due to the dilation. Apparently, these two factors counteract each other, leading to a value of $\Delta\bar{z}_p$ that is nearly independent of ϕ. It is not surprising to see this structural independence with respect to the packing density, given the nearly identical stopping distance, s_d, for all ϕ, evident in Fig. 4. It is also interesting to note that the stopping distance of $s_d \approx 0.55d_l$ for $R = 5$ in Fig. 4 is only slightly less than the value $\Delta\bar{z}_p \approx 0.63d_l$ for the same size ratio in Fig. 13. Obviously, the stopping distance for a fine particles should be within the distance between pore throats as is the case here. Furthermore, these two distances are both slightly less than the large particle diameter, which would be expected for randomly-packed static beds for the ϕ range examined here.

The values of P_p, based on characterizing the pore-throat size distribution using the Delaunay triangulation method, and $\Delta\bar{z}_p$, based on the distance between pore throats along fine particle paths, can be substituted into Eq. 4 for the probability P of a fine particle with size ratio R to penetrate to any particular depth in a random packing with given ϕ. The model's predictions are plotted as solid lines in Fig. 9 and match the DEM results for all cases with various R and ϕ. This indicates that our assumption that free sifting is composed of independent events (i.e., pore-throat sizes are not spatially correlated), which is the basis for the statistical model (Eq. 4), holds. Consequently, the depth of fine particle penetration in the trapping regime depends only on the pore-throat size distribution and the vertical distance between throats.

F. Local percolation velocity

With the pore-throat size distribution and vertical distance between pore throats characterized, it is possible to consider the local percolation velocity in a pore throat as a function of local pore throat size to better understand the similarities in the overall percolation velocity, v_p, between the passing and trapping regimes evident in Fig. 5. First, we define the local percolation velocity as the average vertical velocity of a fine particle with its center within a pore-throat sphere. Then the local percolation velocity, $v_{p,l}$, for a given pore-throat size is averaged over all fine particles within all pore-throat spheres of such size. The vertical velocity outside of the pore-throat spheres, i.e., in the voids, connecting pore-throat spheres, is excluded from the average so that we can associate the local percolation velocity with the pore-throat diameter.

Consider first the case of $R = 7.5$ for the passing regime, shown in Fig. 14(a). The non-dimensional local percolation velocity $-v_{p,l}/\sqrt{gd_l}$ increases with increased d_p/d_f, as would be expected for larger pore throats, and decreases with increased packing density, ϕ, likely due to the associated decrease in the size of the voids between pore-throat spheres. Multiplying $-v_{p,l}/\sqrt{gd_l}$ by ϕ collapses the data [see Fig. 14(b)], much like for v_p, as shown in Fig 5(c). More importantly, the effects of par-

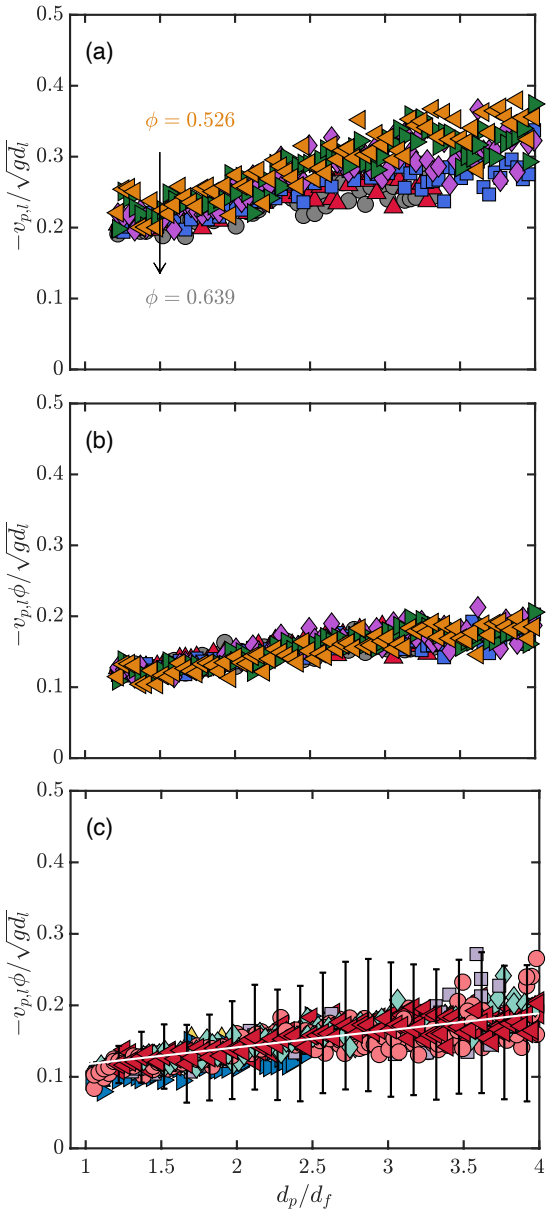

FIG. 14. (a) Non-dimensional local percolation velocity, $v_{p,l}/\sqrt{gd_l}$, vs. pore throat to fine particle size ratio, d_p/d_f, for $R = 7.5$ at various ϕ. Symbols are defined in Fig. 3. (b) Multiplying $v_{p,l}/\sqrt{gd_l}$ by ϕ collapses the data. (c) Additional data for other size ratios, $4 \leqslant R \leqslant 7.5$, both in the trapping and passing regimes with symbols defined in Fig. 5 (a), and the full range of packing densities (not differentiated by symbols) also collapse. Uncertainty bars indicates the standard deviation of the measurement for $\phi = 0.577$ and $R = 7.5$. The white line is a linear fit through the data.

ticle size ratio R are incorporated into the pore throat to fine particle size ratio d_p/d_f, because the pore sizes are directly related to the sizes of the large particles forming the static bed. Consequently, the relationship between $-v_{p,l}\phi/\sqrt{gd_l}$ and d_p/d_f holds for both trapping and passing regimes for all R and collapses all the data for $v_{p,l}$,

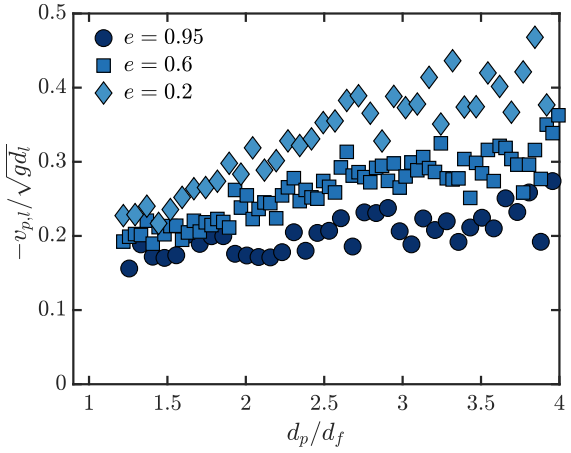

FIG. 15. Non-dimensional local percolation velocity, $v_{p,l}/\sqrt{gd_l}$, vs. pore throat to fine particle size ratio, d_p/d_f, for three restitution coefficients with $R = 7$ and $\phi = 0.577$.

as shown in Fig. 14(c).

The data collapse in Fig. 14(c) makes it possible to predict average percolation velocity for fine particles with various sizes in random packings with different packing densities based on the pore-throat size distribution. The average percolation velocity can be estimated as

$$v_p = \int_1^\infty v_{p,l}(d_p/d_f) P_{psd}(d_p/d_f) \mathrm{d}(d_p/d_f), \qquad (6)$$

where $v_{p,l}(d_p/d_f)$ is obtained by a linear fit to all data in Fig. 14(c), and $P_{psd}(d_p/d_f)$ is the pore-throat size distribution of the entire packing, which is the data from Fig. 12(a) recast as a function of d_p/d_f (based on R) instead of d_p/d_l. The predicted average percolation velocity based on this approach generally deviates from the measured average percolation velocity in Fig. 5 by less than 5% for all of the cases we consider. Thus, it is the local pore throat velocity, $v_{p,l}$, that determines the overall percolation velocity, v_p, whether in the trapping or passing regime.

At this point, we return to the restitution coefficient, which strongly affects the percolation velocity and particle diffusion, as shown in Fig. 8. The impact of e on the local percolation velocity for $R = 7$ and $\phi = 0.577$ is shown in Fig. 15. When the restitution coefficient is large (dark blue symbols), less fine particle energy is dissipated during inter-particle collisions. As a result, fine particles are likely to bounce repeatedly inside pore throats and take a relatively longer time to enter or exit a pore-throat sphere. Consequently, the local percolation velocity increases only slightly with pore-throat size. However, when the restitution coefficient is low (light blue), the kinetic energy of fine particles is largely dissipated in only a single collision. As a result, fine particles fall freely over a longer distance with less bouncing thereby achieving a higher velocity. Consequently, the local percolation velocity for a fine particle with a low restitution coefficient is larger than with a high restitution coefficient, partic-

ularly inside a larger pore-throat sphere. Interestingly, the local percolation velocity for all e values appears to plateau when d_p/d_f is large, analogous to sheared systems where the segregation velocity is nearly independent of size ratio when $R \gtrsim 3$ [8].

Based on the characterization of the local percolation velocity, it is possible to better understand the development of the vertical dispersion of fine particles. First, the particle number distribution in the passing regime is approximately Gaussian [see Fig. 2(b)], which is consistent with the central limit theorem (the sum of independent random variables tends towards a normal distribution even if each original event is not normally distributed). An analogous situation is that the probability distribution for the total distance covered in a two-dimensional random walk (biased or unbiased) becomes a normal distribution given sufficient time [56]. Second, because the local percolation velocity varies more with d_p/d_f for lower restitution collisions (Fig. 15), the distribution of the fine-particle vertical displacement over the same time tends to be wider and, accordingly, yields a larger vertical diffusion coefficient, D_z, than that for higher restitution coefficient, see Fig. 8(b).

IV. CONCLUSIONS

The percolation of fine intruder particles in static random packings of identical large particles depends on the particle size ratio, packing density, and restitution coefficient. Unlike previous studies, we consider both dynamic features of the fine particle motion and static features of the large particle bed for free sifting with an intermediate particle size ratio, $4 \leqslant R \leqslant 7.5$, which encompasses conditions both above and below the geometric trapping threshold, $R_t = 6.464$ [14].

For these size ratios, R_t determines whether a fine particle is trapped or not, leading to the passing and trapping regimes (Fig. 2). However, no sharp transitions for the percolation velocity and diffusion coefficients (or Péclet numbers) between these two regimes are evident, even when the size ratio is as low as 4, where most fine particles are quickly trapped, or when the packing density approaches the random close packing limit (Fig. 5). In fact, when scaled properly, the percolation velocity is invariant across a fairly large range of size ratios and packing densities for both passing and trapping regimes [Fig. 5(c)], a surprising result. Likewise, the scaled local percolation velocity in individual pore throats depends on the local pore throat size and packing density but is independent of whether the percolation is in the trapping or passing regime [Fig. 14(b)]. This relationship [informed by Fig. 14(c)] can be used to predict the overall percolation velocity for a wide range of R and ϕ. The restitution coefficient, e, also affects the dynamics of free sifting significantly. The local percolation velocity as a function of local pore-throat size decreases as e increases and demonstrates less variation (Fig. 15), which in turn results in smaller overall percolation velocity and smaller diffusion coefficients (Fig. 8). Both of these effects result from the more energetic interactions between the fine particle and bed particles that occur at larger e, where the fine particle may bounce repeatedly in a pore before passing through it.

In the trapping regime, the probability that a fine particle is trapped at a particular depth follows a simple relationship, suggesting that free sifting in a static bed is a process consisting of independent sievings. The dependence of the probability on particle size ratio and packing density can be understood by characterizing the pore structure of the static bed using the modified Delaunay triangulation method (L1). The structural information informs the passing probability P_p and the average vertical distance between pore-throat spheres $\Delta\bar{z}_p$, upon which the model to predict the probability for a fine particle to reach any depth is based. Similarly, characterizing pore-throat size distributions makes it possible to understand their influence on the local percolation velocity, which determines the overall percolation velocity. We also note that for static beds prepared using other packing approaches, e.g., settling large bed particles under gravity or freezing flowing large particles, our approach for predicting the percolation depth remains accurate, even though the pore statistics, such as the passing probability and the pore size distribution, can vary at similar packing densities.

In addition to providing a better understanding of fine particle percolation in static particle beds, these results provide a framework that can be extended to sheared flows of fine and large particles. While size segregation due to percolation in granular flows has been successfully characterized for $R \lesssim 3$ [3, 4, 7, 8], the nature of the segregation seems to change at larger R. This has been attributed to free sifting [8], but with the caveat that free sifting would be expected to occur near $R_t = 6.464$, a much larger size ratio than that where the dominant physics of size segregation changes. However, the results in this study demonstrating that significant percolation occurs in static beds at size ratios as small as $R = 4$, albeit in the trapping regime, suggest that it is reasonable that free sifting alters the physics of size segregation in flowing granular mixtures at size ratios well below R_t. In fact, one could argue that the continuous opening of voids in the flowing granular material might be analogous to decreasing the packing density under the static bed conditions considered here. Even so, it is clear that the problem of fine particle percolation in flowing granular materials is more complicated than that in a static bed and deserving of further study.

ACKNOWLEDGMENTS

We are grateful for insightful discussions with John Hecht and Yi Fan. This work is supported by the National Science Foundation under Grant No. CBET-

2203703.

[1] H. M. Jaeger, S. R. Nagel, and R. P. Behringer, Rev. Mod. Phys. **68**, 1259 (1996).
[2] J. Duran, *Sands, powders, and grains: an introduction to the physics of granular materials* (Springer Science & Business Media, New York, 2012).
[3] J. M. N. T. Gray, Annu. Rev. Fluid Mech. **50**, 407 (2018).
[4] P. B. Umbanhowar, R. M. Lueptow, and J. M. Ottino, Annu. Rev. Chem. Biomol. Eng. **10**, 129 (2019).
[5] J. C. Williams, Powder Technol. **2**, 13 (1968).
[6] J. Drahun and J. Bridgwater, Powder Technol. **36**, 39 (1983).
[7] S. Savage and C. Lun, J. Fluid Mech. **189**, 311 (1988).
[8] C. P. Schlick, Y. Fan, A. B. Isner, P. B. Umbanhowar, J. M. Ottino, and R. M. Lueptow, AIChE J. **61**, 1524 (2015).
[9] C. Bemrose and J. Bridgwater, Powder Technol. **49**, 97 (1987).
[10] D. Schulze, *Powders and bulk solids: Behaviour, characterization, storage and flow* (Springer, Berlin, 2008).
[11] J. C. Phillips, A. J. Hogg, R. R. Kerswell, and N. H. Thomas, Earth Planet. Sci. Lett. **246**, 466 (2006).
[12] E. Linares-Guerrero, C. Goujon, and R. Zenit, J. Fluid Mech. **593**, 475 (2007).
[13] R. Chassagne, P. Frey, R. Maurin, and J. Chauchat, Phys. Rev. Fluids **5**, 114307 (2020).
[14] J. Dodds, J. Colloid Interface Sci. **77**, 317 (1980).
[15] I. Ippolito, L. Samson, S. Bourles, and J.-P. Hulin, Eur. Phys. J. E **3**, 227 (2000).
[16] F. Lominé and L. Oger, Phys. Rev. E **79**, 051307 (2009).
[17] M. M. Roozbahani, L. Graham-Brady, and J. D. Frost, Int. J. Numer. Anal. Methods Geomech. **38**, 1776 (2014).
[18] A. Kerimov, G. Mavko, T. Mukerji, and M. A. Al Ibrahim, Phys. Rev. E **97**, 022907 (2018).
[19] C. Ghidaglia, L. de Arcangelis, J. Hinch, and É. Guazzelli, Phys. Rev. E **53**, R3028 (1996).
[20] J. Bridgwater, N. Sharpe, and D. Stocker, Trans. Inst. Chem. Eng. **47**, 114 (1969).
[21] J. Bridgwater and N. Ingram, Trans. Inst. Chem. Eng. **49**, 163 (1971).
[22] J. Masliyah and J. Bridgwater, Trans. Inst. Chem. Eng. **52**, 31 (1974).
[23] P. Richard, L. Oger, J. Lemaître, L. Samson, and N. N. Medvedev, Granul. Matter **1**, 203 (1999).
[24] F. Lominé and L. Oger, J. Stat. Mech. Theory Exp. , P07019 (2006).
[25] M. Rahman, H. Zhu, A. Yu, and J. Bridgwater, Particuology **6**, 475 (2008).
[26] H. Zhu, M. Rahman, A. Yu, J. Bridgwater, and P. Zulli, Miner. Eng. **22**, 961 (2009).
[27] J. Li, A. Yu, J. Bridgwater, and S. L. Rough, Powder Technol. **203**, 397 (2010).
[28] S. Remond, Phys. A: Stat. Mech. Appl. **389**, 4485 (2010).
[29] P. A. Cundall and O. D. Strack, Geotechnique **29**, 47 (1979).
[30] D. W. Mellor, *Random close packing (RCP) of equal spheres: structure and implications for use as a model porous medium* (Open University, United Kingdom, 1989).
[31] R. Al-Raoush, K. Thompson, and C. S. Willson, Soil. Sci. Soc. Am. J. **67**, 1687 (2003).
[32] N. Reboul, E. Vincens, and B. Cambou, Granul. Matter **10**, 457 (2008).
[33] F. Seblany, E. Vincens, and C. Picault, Int. J. Numer. Anal. Methods Geomech. **45**, 1195 (2021).
[34] A. B. Isner, P. B. Umbanhowar, J. M. Ottino, and R. M. Lueptow, Chem. Eng. Sci. **217**, 115505 (2020).
[35] A. B. Isner, P. B. Umbanhowar, J. M. Ottino, and R. M. Lueptow, AIChE J. **66**, e16912 (2020).
[36] J.-S. Lee, M. Guimaraes, and J. C. Santamarina, J. Geotech. Geoenviron. Eng. **133**, 1136 (2007).
[37] M. Suzuki, T. Shinmura, K. Iimura, and M. Hirota, Adv. Powder Technol. **19**, 183 (2008).
[38] B. D. Lubachevsky and F. H. Stillinger, J. Stat. Phys. **60**, 561 (1990).
[39] S. Torquato, T. M. Truskett, and P. G. Debenedetti, Phys. Rev. Lett. **84**, 2064 (2000).
[40] S. Torquato and F. H. Stillinger, Rev. Mod. Phys. **82**, 2633 (2010).
[41] M. Jerkins, M. Schröter, H. L. Swinney, T. J. Senden, M. Saadatfar, and T. Aste, Phys. Rev. Lett. **101**, 018301 (2008).
[42] G. D. Scott and D. M. Kilgour, J. Phys. D: Appl. Phys. **2**, 863 (1969).
[43] C. Song, P. Wang, and H. A. Makse, Nature **453**, 629 (2008).
[44] R. Besseling, E. R. Weeks, A. Schofield, and W. Poon, Phys. Rev. Lett. **99**, 028301 (2007).
[45] N. Menon and D. J. Durian, Science **275**, 1920 (1997).
[46] S. Hsiau and M. Hunt, J. Fluid Mech. **251**, 299 (1993).
[47] B. Utter and R. P. Behringer, Phys. Rev. E **69**, 031308 (2004).
[48] D. Wilkinson and S. F. Edwards, Proc. Math. Phys. Eng. Sci. **381**, 33 (1982).
[49] Uncertainty bars represent two standard deviations of the uncertainty associated with the finite sample sizes used to compute P, i.e., $\pm\sqrt{n_p}/N$, where n_p is the number of particles passing the associated depth and N is the total number of particles.
[50] C. Ghidaglia, E. Guazzelli, and L. Oger, J. Phys. D **24**, 2111 (1991).
[51] C. Ghidaglia, L. de Arcangelis, J. Hinch, and E. Guazzelli, Phys. Fluids **8**, 6 (1996).
[52] P. Meakin and R. Jullien, J. Phys. **51**, 2673 (1990).
[53] V. Luchnikov, N. Medvedev, L. Oger, and J.-P. Troadec, Phys. Rev. E **59**, 7205 (1999).
[54] L. Sarkisov, R. Bueno-Perez, M. Sutharson, and D. Fairen-Jimenez, Chem. Mater. **32**, 9849 (2020).
[55] H. Dörrie, *100 great problems of elementary mathematics* (Courier Corporation, New York, 2013).
[56] I. D. Dinov, N. Christou, and J. Sanchez, J. Stat. Educ. **16** (2008).